Geotectonics, Vol. 37, No. 3, 2003, pp. 245–260. Translated from Geotektonika, No. 3, 2003, pp. 79–96.

Thermal Tomography of the West Arctic Basin

M. D. Khutorskoi*, L. V. Podgornykh, I. S. Gramberg**†, and Yu. G. Leonov***

**Geological Institute (GIN), Russian Academy of Sciences, Pyzhevskii per. 7, Moscow, 119017 Russia*
***All-Russia Research Institute of Geology and Mineral Resources of the World Ocean (VNIIOkeanologiya), Angliiskii pr. 1, St. Petersburg, 190121 Russia*

Received March 14, 2002

Abstract—Geothermal modeling of the nonstationary thermal field in the crust and the lithosphere was carried out along 123 seismic tomography geotraverses across the Barents and Kara seas and the Eurasian sector of the Arctic Ocean. The thermal structure of the lithosphere in the geologic past and at present was deduced. Three-dimensional temperature and heat flow distribution models were compiled in the latitude–longitude–depth coordinates. The depth to the oil window was estimated. Paleotemperatures were determined for the period when the principal offshore oil fields were formed, and the relationship between oil field locations and heat flow distribution was detected.

The geologic and economic significance of West Arctic seas is due to giant oil and gas resources in offshore sedimentary basins and is likely to increase with the development of the already known HC fields and the discovery of new.

The lack of investment into costly offshore seismic surveys raises the practicability of the relatively cheap methods of indirect petroleum potential estimation based on available geologic and geophysical data.

One such method is the thermal tomography of the crust based on three-dimensional geothermal modeling. Three-dimensional (volumetric) temperature and heat flow distribution modeling enables researchers to examine geothermal maps for various depth slices and thereby determine the depth to the oil window, that is, to predict possible depths and locations of the existing oil fields.

Offshore geothermal surveys on the shelf of the Eurasian basin of the Arctic Ocean began in the 1970s with measurements made by PTG-3M immersible probes in the Barents Sea [7]. These measurements were made on the shelf in seawater at depths of up to 300 m with a one-channel probe immersed in sediments to a depth of two meters at the most. As expected, the data obtained demonstrated a strong influence of exogenic thermal fields upon the interior heat flow intensity, in particular, seasonal seafloor temperature variations depending on insulation and rapid bottom currents bringing water masses with contrasting (relative to local background) temperatures. This factor was particularly obvious in the southern sector of the sea within the scope of the warm Nordkapp stream. As a result, conditional background heat flow values could not be obtained from probe measurements, because the latter varied over a fairly wide range, from 0 to more than 500 mW/m^2, and did not adequately reflect the spatial distribution of deep-seated thermal sources.

During the active HC exploration campaign that began in the 1980s, well logging, including temperature logging, was carried out in offshore and island-based exploratory wells. The first downhole heat flow measurements in the southern Kara Sea were made simultaneously. Temperature measurement processing provided temperature gradient estimates, and the thermal conductivities of rocks were determined in core samples by thermal analysis. As a result, conditional heat flow values were obtained for the first time in the region [17]. However, downhole temperature measurements were too sparse for such a vast area and therefore insufficient for temperature and heat flow distribution mapping, let alone for the calculation of subsurface temperatures in the lithosphere of the region.

THERMAL FIELD MODELING METHOD

We have worked out a method for the 2D and 3D modeling of a non-stationary thermal field to estimate temperatures at depths that are not penetrated by drilling and the depth of the oil window. The thermal medium, including the configurations of thermally contrasting layers and thermal conductivity and diffusivity values, were preset by digitizing structural units recognized from seismic data acquired along 123 geotraverses (Fig. 1). Heat flow values measured in wells were used as end values. The 67 wells in the Barents Sea, where the heat flow values were measured, were spaced in such a way that at least one well was located within a DSS (wideangle deep seismic profiling) swath. Three wells in the southern Kara Sea were located along the longest seismic line (Fig. 2).

Deep subsurface temperatures along the seismic lines were calculated using the TERMOGRAF soft-

†Deceased.

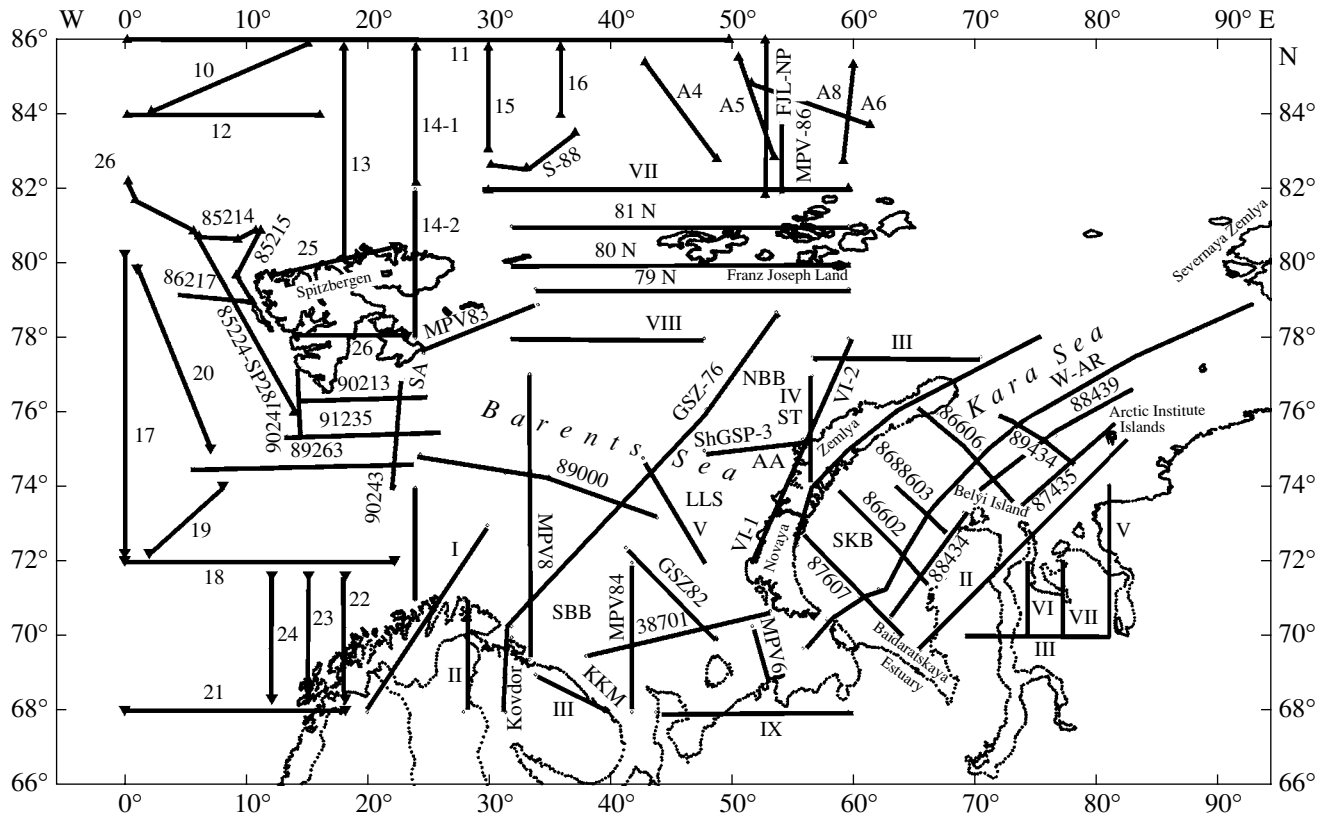

Fig. 1. Location and indices of seismic geotraverse lines in the Western Arctic. Abbreviations: SBB—South Barents Basin, NBB—North Barents Basin, LLS—Ludlov–Lunin saddle, AA—Admiralteiskii arch, ST—Sedov trough, KKM—Kola–Kanin monocline, SA—Svalbard anteclise, SKB—South Kara Basin, FJL—Franz Joseph Land, NP—North Pole, MPV—refraction seismic line, ShGSP—wide-angle deep seismic profile, GSZ—DSS, W-AR —West Arctic seismic line.

ware [15]. The calculations were based on the thermal properties of crustal layers in compliance with the established refractor velocities (table).

Temperature distribution in the sequence was deduced using the finite element method with a quadratic approximation of the temperature function between the junctures of a rectangular grid. The program provides for a grid of 41×41 junctures (that is, a two-dimensional problem is solved) whose linear dimensions along the X and Z axes can be changed by the operator. Lateral flow is assumed to be absent at the lateral boundaries of the modeling domain, that is, $\partial T/\partial x = 0$. We assumed the temperature at the seafloor–water interface known from meteorological data (~1°C) to be the upper end value and heat flow to be the lower end value.

Inside the modeling domain, contrasting media configurations and their thermal properties, including thermal diffusivity a (m^2/s), thermal conductivity k (W/(m K)), and normalized thermal source density ($Fi = A/(c\rho)$) (K/s), were preset. Within the TERM program, which is responsible for calculations, the linear dimensions (Lx and Lz, km) of the modeling domains were preset to determine the linear dimensions of the junctures (Lx/41 and Lz/41) as well as the solution discretization interval (Ma). The time step of the iteration process was selected automatically by the program and calculated as $\tau = 10^{-7}(Z^2/4a)$, where Z is the thickness of the modeling domain.

As a result of the digital solution of the thermal conductivity equation, temperate and heat flow distribution $q(z)$ and $q(x)$ for the preset thermal medium at the final moment of the discretization phase were obtained. The file of results was renamed as the file of initial temperatures, and calculations in the next phase begin with the final moment of the previous step. Solution discretization is convenient when it is necessary to introduce changes into the thermal medium in response to structural and material changes in geologic sequence, to preset the distribution of new thermal sources and discharge zones, and to revise estimated paleothermal field parameters. If heat and mass transfer must be included in the model, it can be imitated by presetting end temperature values and/or adiabatic gradients in the depth interval covered by convection.

For each profile, the end temperature value was taken at the upper boundary and the heat flow value, at the lower boundary (q_{bd}) in compliance with the value measured in the nearest well (q_{obs}) minus heat flow generated in the crustal layer above the lower boundary of

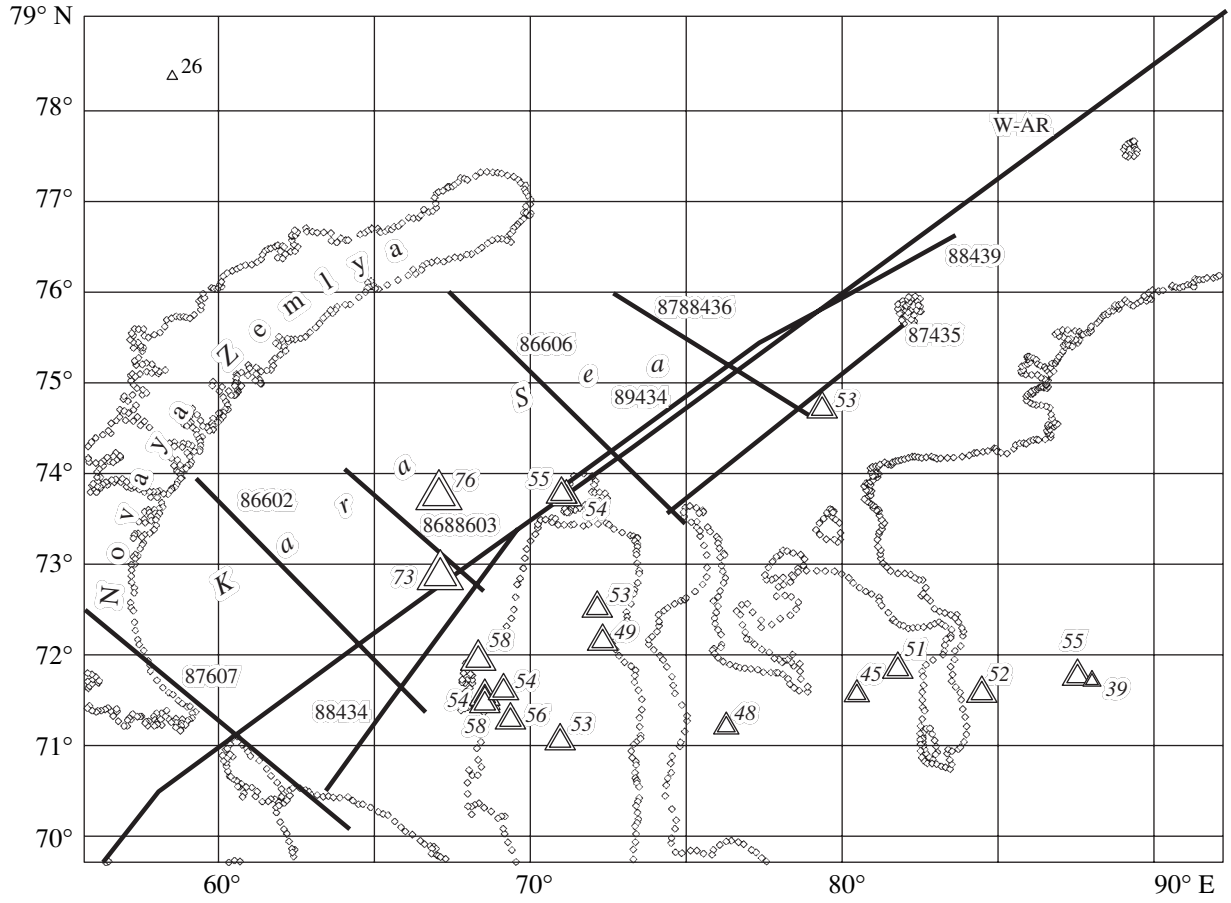

Fig. 2. Locations of wells (triangles) in the Kara Sea region where downhole thermometry was carried out. Triangle sizes are proportionate to heat flow values (mW/m^2).

the modeling domain as a result of the spontaneous decay of long-lived radioactive isotopes (q_{est}), that is,

$$q_{bd} = q_{obs} - q_{est}.$$

The latter was estimated from layer thickness and composition as deduced from seismic data using the standard specific heat values for respective rock types: $(q_{est})_i = A(x, z)z_i$ [10]. The reduced end heat flow values varied within 30–40 mW/m^2 from one region to another.

The initial conditions for temperature calculation in most profiles were preset for a time of 60 Ma. By that time, as is obvious from the paleotectonic reconstructions of the Barents Sea basin [5, 14], the present-day crustal structure had already been formed, and heat flow evolution, even if it took place, was related to the relaxation of initial thermal heterogeneities rather than a reformation of the structural–thermal pattern.

Under such terminal conditions, the temperatures within the modeling domain rapidly reached a stationary state, which was adopted a priori as a criterion of calculation correctness. The duration of time steps was 10 Ma. Within the time interval 60–0 Ma, therefore, we made six control steps to check the stationary-state conditions. Modeling data showed that all the profiles demonstrated stationary thermal fields starting from the third step, that is, 30 Ma after the start of the calculation.[1]

Calculation accuracy was estimated by two criteria: firstly, the match of model and measured heat flow values and, secondly, the match of temperatures at line crossings. The error of isotherm occurrence depth, estimated by the least squares method, was ±150 m, or 0.5% for a calculation depth of up to 30 km.

Three-dimensional geothermal modeling in the region was carried out using the three-dimensional graphic software TECPLOT v. 7.0-demo (Amtec Engineering Inc.), which enabled three-dimensional interpolation of the observed field (in our case, temperature, heat flow, and structural boundaries deduced from seismic tomography) in latitude–longitude–depth coordinates. A special file preparation program was created in TECPLOT v. 7.0 format, which transformed text files with thermal modeling results into TECPLOT database format provided that the terminal coordinates of the

[1] In subsequent calculations, there were reasons to adopt a time step of 20 Ma.

Thermal parameters preset for crustal thermal field modeling

Formation/Parameter		Refractor velocity, km/s	Thermal diffusivity $a \times 10^{-7}$, m^2/s	Thermal conductivity k, W/(m K)	Heat generation (normalized), $Fi \times 10^{-13}$ K/s
Nonconsolidated sediments		<3.7	3.0	1.3	–
Consolidated Mesozoic–Cenozoic clastics			3.5	1.5	–
Paleozoic carbonates		4.7	3.8	1.9	1.5
Granites	upper part,	6.0	5.0	2.5	5.52
	lower part	6.5	5.0	2.5	3.5
Basalts, mixed crustal–mantle rocks		>6.5	7.0	2.9	–
Crustal ultramafics		–	8.0	3.0	–
Mantle ultramafics		–	10.0	3.2	–

Note: a is thermal diffusivity; k, thermal conductivity; Fi, the normalized heat generation value (A), $Fi = \frac{A}{c\rho}$, where c is specific heat and ρ is density.

seismic line and the vertical spacing step were preset. This program enabled three-dimensional interpolation for any grid configurations. In our case, we used an irregular grid tied-up to seismic line orientations, along which two-dimensional estimations of deep subsurface temperature were carried out.

THE THERMAL EVOLUTION OF THE REGIONAL LITHOSPHERE

Heat flow changes in time are discussed below with reference to the thermal evolution of the lithosphere along the trans-Barents geotraverse (GSZ-76 line) (Fig. 1), which crosses most of the crustal structures recognized from seismic data in the Barents Sea platform and is obviously most informative. The thermal field was calculated for the geologic time span from 300 Ma to the present day. This problem was solved with due regard for the effects of all of the established tectonic events upon interior thermal conditions.

The initial modeling conditions were preset for a time of 300 Ma (Middle Carboniferous), when the inception of the NW-trending southern rift broke the continuity of the Proterozoic continental crust in the southern Barents Sea, as is clear from geologic data [14, 18]. Since the Riphean, the basin accommodated clastic and carbonate sedimentation at progressively growing rates, which acquired the mode of avalanche sedimentation in the mid-Paleozoic. This process eventually led to the accentuation of the Paleozoic upper carbonate complex, which can be recognized from CDP seismic data. This complex is characterized by P-wave velocities of 5.4–5.8 km/s and exhibits maximum thickness (up to 12 km) in the interval of 450–600 km from the start point of the seismic line (near Murmansk). Below this complex are the blocks of the granite–metamorphic layer with interval velocities of 6.0–6.5 km/s and a thickness of 22–23 km, which correlate with the Archean–Lower Proterozoic granites and host rocks of the Baltic shield. This layer thins out abruptly at a distance of 500 km from the start point, where the crust acquires a suboceanic structure. Judging from seismic data, the proportion of basalts and hyperbasites relative to granites and metamorphic rocks and the thickness of Mesozoic–Cenozoic sediments gradually increase northeastward. Crustal thickness decreases northward from 40 to 35 km [13]. Lithospheric thickness was not estimated from seismic data, but theoretically and by analogy with other continent–ocean transition zones, it decreases northward from 150 km in the southern part of the profile down to 100–120 km.

The lithospheric sequence preset for this time slice consisted of four thermal layers [11]. The lowermost was the "upper-mantle" layer with a thermal diffusivity of 10^{-6} m^2/s and a thermal conductivity of 3.2 W/(m K). The thickness of this layer was 100 km. Above it was the "mixed crustal–mantle" layer with a thickness of 15 km, an assumed thermal diffusivity of 8×10^{-7} m^2/s, and a thermal conductivity of 2.9 W/(m K). The granite–metamorphic layer was characterized by a thermal diffusivity of 5×10^{-7} m^2/s and a thermal conductivity of 2.5 W/(m K). These values, which are typical of the respective rock types, were conventionally preset in all thermal models. Within this model, the uppermost layer of consolidated carbonate sediments was characterized by a thermal diffusivity of 4×10^{-7} m^2/s and a thermal conductivity of 2.3 W/(m K). The model was compiled on the basis of first-kind terminal conditions: the temperature was assumed to be 1°C on the surface (bottom water temperature) and 1250°C at the base of the lithosphere. Radiogenic heat generation in the granite–metamorphic layer and rift-related heat generation in the mantle were taken into account for respective pro-

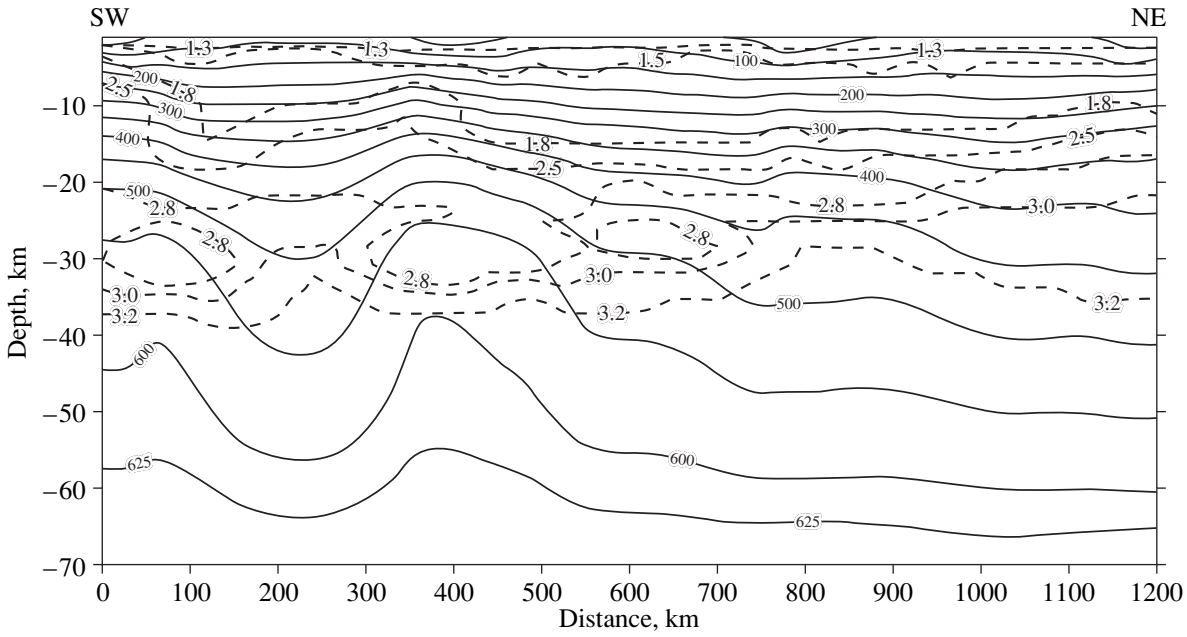

Fig. 3. Temperature profile (°C, solid lines) and thermal conductivity distribution (W/m K, dashed lines) along the GSZ-76 line for the time slice of 120 Ma.

file intervals[2] (*Fi*). The source intensity was preset as normalized to the ($c\rho$) values of rocks, that is, $Fi = A/(c\rho)$, where A is heat generation intensity in unit volume (W/m^3). The radiogenic heat value was determined from the measured concentrations of long-lived ^{238}U, ^{232}Th, and ^{40}K isotopes in the rocks of the Baltic shield [1], and its normalized power *Fi* was taken to be 3.5×10^{-13} K/s. The normalized power of the rift-related source (asthenospheric plume) was estimated on the assumption that it was the same during the Late Paleozoic as in modern continental rift zones, such as Lake Baikal [6], the Rio Grande rift [20], or the Kenya rift zone [21]—12×10^{-13} K/s. The initial temperatures in the model were calculated by solving the Poisson's unidimensional stationary equation for a stratified model with only radiogenic interior heat sources and using the thermal characteristics and thicknesses of rocks as mentioned above. The rift-related thermal source was included during the first phase of modeling. The time step during the first phase of modeling was 50 Ma, which means that the fulfillment of the first step provided the thermal structure of the lithosphere for the time slice of 250 Ma (earliest Late Permian). The obtained temperatures in the lithospheric sequence were assumed to be the initial temperatures for the next phase of nonstationary process calculation for an equal period of 50 Ma, but now the rift-related source was excluded, because continental rifts do not exist longer than 40 Ma [8] and, most probably, not even longer than 30 Ma. After the second step, the model reflected the thermal conditions for the time slice of 200 Ma (the Middle to Late Triassic).

During this step, the modeling parameters were changed. Whereas the sequence in the former two time steps included the whole lithosphere, the lower boundary of the sequence for the time slice of 200 Ma was limited to a depth of 70 km, as established from DSS data. The heat flow value determined during the previous calculation phase was preset for this depth. It ranged within 34 to 40 mW/m^2 along the profile.

In crustal section, the geologic structure was reflected in more detail. The model reflected the block structure of the sequence expressed as the subvertical of the contacts between the granite–metamorphic complex and the metamorphosed Paleozoic sediments and basalts and hyperbasites in the southwestern part of the profile (interval 100–200 km) (Fig. 3). These blocks contact along faults or flexure zones initiated not later than the Middle Paleozoic, as is obvious from the ages of the sedimentary rocks. The age of deformations suggests the absence of modern permeability zones capable of accommodating heat and mass transfer; therefore, the faults and flexures were modeled merely as boundaries between contrasting thermal media.

As a result of thermal modeling with a step of 80 Ma, the temperature distribution pattern in the crust of the Barents Sea region was obtained for the time slice of 120 Ma (the Early to Late Cretaceous) (Fig. 3). Noteworthy are two isotherm distortion zones in the intervals 0–150 and 300–500 km from the start point of the seismic line. They are related to the presence of isolated granite–metamorphic rock lenses among mafic

[2] The shape of the anomalous rift-related heat source was associated with an asthenospheric plume (asthenolith).

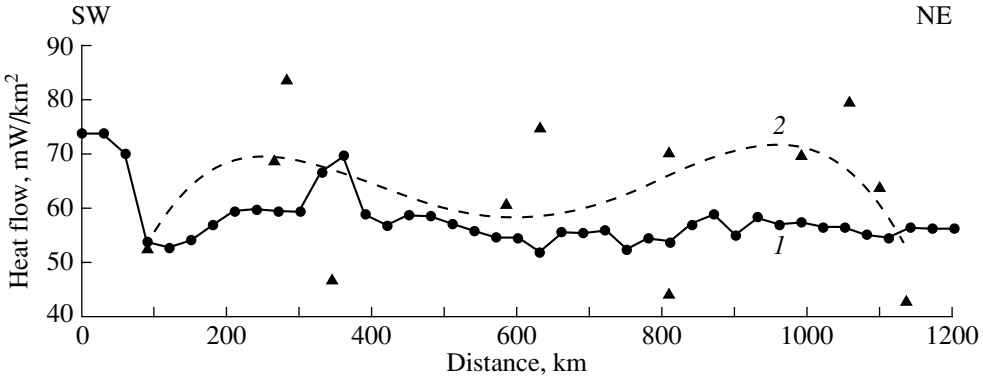

Fig. 4. Heat flow profiles along the GSZ-76 geotraverse: *1*—model heat flow, *2*—averaged measured heat flow. Triangles indicate the observed values.

rocks. The lower thermal conductivity of granites relative to basalts and ultramafic rocks and the complex bedding geometry in the sequence resulted in heat flow refraction. Heat flow density decreases on the edges of bodies with low thermal conductivities because of the streamline effect but increases between such bodies, because heat flows tend to propagate along the lines of least resistance. This phenomenon is well known from the potential theory and does not require further explanation. It is clearly expressed in the geothermal fields of many geologic bodies [15]. Note that virtually all the heat flow distortions revealed by the models originate from the structural and thermal heterogeneities of the sequence (Fig. 4, curve *2*). The effect of seafloor topography as the factor inducing isotherm and heat flow distortions is negligible for this profile as compared with the effect mentioned above.

Paleotemperature and heat flow evaluation for this time slice is particularly important for predicting the depth and configuration of oil and gas accumulation zones, considering that the oils in the southern Barents Sea are dated as Late Jurassic–Early Cretaceous.

The next time step was calculated for a time of 60 Ma (Eocene). Besides the ongoing clastic sedimentation, no structural reformation events occurred. But the rate of sedimentation during this period was so low[3] that the process, according to our calculations, did not distort the heat flow. Consequently, the thermal field at that time reflected relaxation after the impact of the Late Paleozoic thermal source only. The temperature and heat flow distribution pattern for that period was similar to the pattern obtained for 120 Ma. This suggests that the geothermal field became quasi-stationary, i.e., ceased to evolve with time. Maturity isotherms (110 and 160°C) remained at the same depth as after the previous time step, that is, 4–5.5 km and 4.5–6.5 km. To summarize, the stationary thermal field in this region was established approximately by the end of the Mesozoic. This is supported by geologic evidence [5] indicative of the inception of postrift evolution over the whole Barents–Kara platform during the Jurassic–Late Cretaceous, when rifting continued beyond its limits.

The present-day thermal structure was obtained within the next time step (0 Ma). The estimated surface heat flow profile repeats the bend of the isotherms (Fig. 5). It acquires peak values of 65–67 mW/m^2 in the interval L = 500–700 km above granite–metamorphic basement highs that rise up to 4–6 km below the seafloor, according to seismic data. The modeled background heat flow value is 54 mW/m^2. This value was estimated by averaging heat flow values calculated along the profile [15].

The heat flow trend was not detected along this profile. The heat flow values were virtually constant except those of the two zones mentioned above. However, Tsybulya and Levashkevich [17] indicate the existence of a heat flow trend: these authors believe that it grows northward. In all probability, the specific features of heat flow distribution were misinterpreted by these authors based on the analysis of measured values distorted by surficial thermal impact.

It is appropriate at this point to comment on the difference between the observed (67–75 mW/m^2, Fig. 4) and calculated (model) heat flows. Heat flow values along the trans-Barents geotraverse were measured on the shelf or relatively shallow abyssal plains. The experience of such measurements [19, 22, 23] suggests that the exogenic distortions of heat flow may take place in up to 1–1.2 km of seawater or even deeper if bottom currents are present. The effect of exogenic factors can be detected indirectly from the extremely high dispersion of the observed heat flow values, from zero to 594 mW/m^2. Such a wide variation cannot be due to subsurface thermal sources, and we can only attribute it to the effect of exogenic distorting factors such as the effect of seasonal seafloor temperature variations, changes in the hydrological situation (nonstationary bottom currents), and secular temperature variations

[3] According to [5], the rate of sedimentation within the platform-type Barents Sea crust at 60 Ma was 3×10^{-2} mm/yr. With such sedimentation rates, heat flow may only experience insignificant alterations, which do not exceed measurement error.

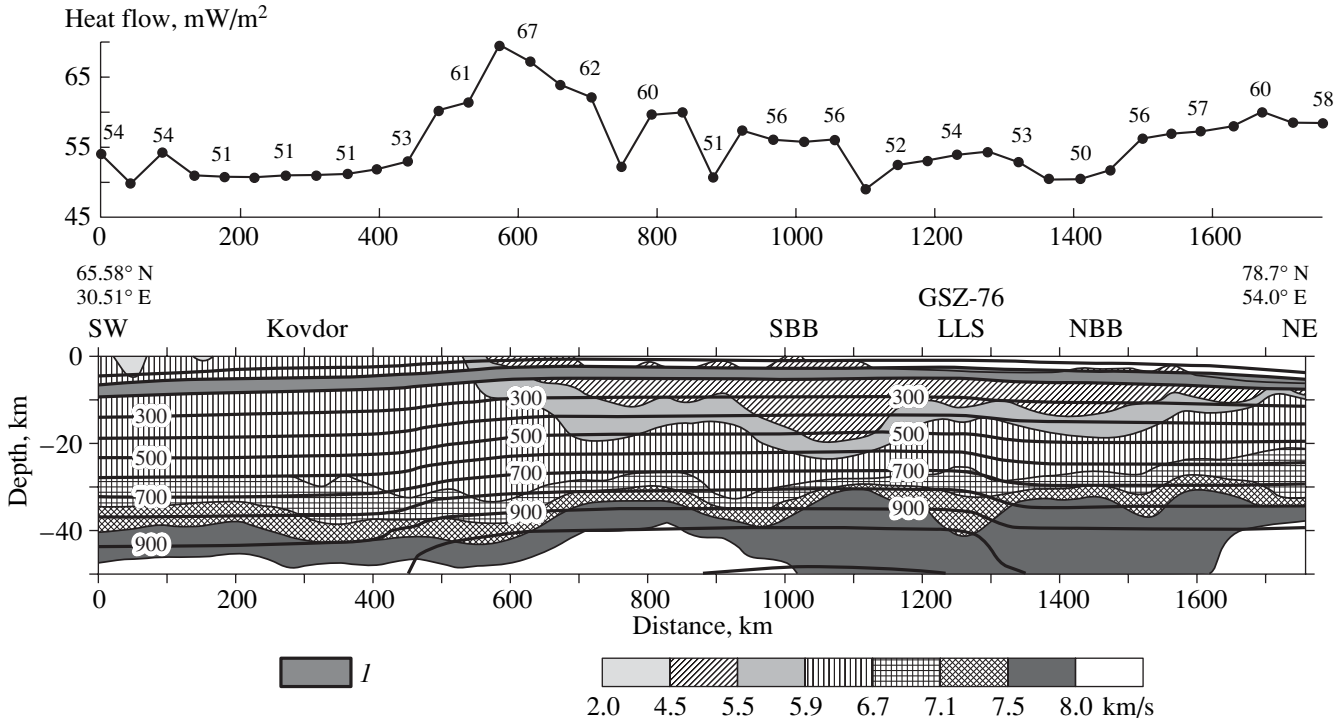

Fig. 5. Seismic tomography (refractor velocities, km/s) and temperature (isotherms, °C) profiles along the Kovdor and GSZ-76 lines with a heat flow profile in the upper part. (*1*) Oil window.

(paleoclimatic effect). We can only detect these distorting factors qualitatively from the wide dispersion of measured heat flow values. Their quantitative estimation can only be made on the basis of temperature regime observations, bottom current rate and temperature measurements, and hydrogeological data on groundwater dynamics. In shallow waters, the only way to obtain reliable empirical heat flow values is to measure them in exploratory wells, where the magnitude of the exogenic temperature wave effect is lower than the temperature measurement error.

The benchmark for comparisons between measured and modeled heat flow values along the trans-Barents geotraverse are the geothermal measurements made in Well SG-3 in the Pechenga trough and in wells drilled on islands in the Barents Sea. Measurements in Well SG-3 were made by high-precision devices under equilibrium (settled) temperatures in the hole; the measurements were repeated several times and accompanied by measurements in satellite wells [3, 9]. Also, the thermal section of the Kola superdeep well was studied in detail [2]. Therefore, the heat flow values measured in this well can be regarded as a benchmark for comparisons with model geothermal data on the southwestern end of the profile. The heat flow value measured in the upper 7 km of the hole ranges within 38–40 mW/m^2. Deeper than 7 km, the measured heat flow value gradually grows up to 50–55 mW/m^2. These values are considered to be adequate to the background heat flow value, and its decrease in the upper part of the sequence is attributed largely to changes in downhole hydrodynamics and, to a lesser extent, to the effect of paleoclimatic variations. Therefore, the model surficial heat flow values agree well with the background heat flows estimated in Well SG-3. Note that similar heat flow values are characteristic of the whole wedge of continental crust. It follows that if the structural and thermal sections preset for modeling are true, the estimated heat flow values along the profile are also close to real values. The match of modeled and measured heat flow values has also been detected in wells drilled on Kolguev Island, where heat flow values of 44–48 mW/m^2 were established in wells Bugrinskaya and Peschanoozerskaya 3 and 52 mW/m^2, in well Peschanoozerskaya 1 [17]. Although these wells are located outside the profile under consideration, these data attest to the correctness of the background heat flow estimates.

To summarize, the background heat flow value in the Barents Sea is higher than the heat flow characteristic of the Precambrian structures of the Baltic shield. This is due to the younger (Riphean–Paleozoic) age of rift-related thermal sources beneath the sea as compared with the adjacent land and, consequently, the later cessation of active tectonic and thermal processes.

GEOTHERMAL MODELING ALONG THE MAIN GEOTRAVERSES

Geothermal modeling was conducted along a network of seismic tomography lines in the Barents [16]

and Kara [12] seas and the western part of the Eurasian sector of the Arctic Ocean (Fig. 1).

The thermal properties of the layers and modeling parameters mentioned above were universal for all the profiles because of the universal seismic velocities and uniform interpretation of seismic tomography data for these sequences.

Deep seismic profiling from two vessels (wideangle deep seismic profiling) for the first time provided reliable data on the structure of the whole crust from top to bottom. It is important that, unlike DSS, refraction, and stratigraphic drilling data, the reflectors and, consequently, the interfaces between contrasting media were traced continually.

Besides new data on the structure of the Barents–Kara shelf platform, deep seismic profiles demonstrated the reliability, that is, the consistency of these data with the real situation. The match of interpreted seismic data, even in details, at the crossings provides additional evidence for the truth of the data obtained.

The Kovdor-GSZ-76 profile provides the most complete data on the structure of the Barents Sea region as a whole, because it is the longest and crosses the whole sea from southwest to northeast, from the Kola Peninsula to the Franz Joseph Land Archipelago (Fig. 5). The length of the profile is more than 1300 km [13].

As is obvious from the profile, the sequence beneath the Barents Sea floor encompasses the whole Phanerozoic and exhibits maximum thickness and completeness in the South and North Barents basins together with the Ludlov–Lunin saddle between them. The maximum thickness of the Phanerozoic sequence has been detected in the South Barents Basin (up to 22 km). Somewhat lesser thicknesses (up to 18 km) were estimated on the saddle and in the North Barents Basin. The thickness of the fill decreases rapidly on the flanks of the Barents megabasin. Within the Franz Joseph Land, it is as thin as 10–11 km. Moreover, the bulk of the sequence is represented here by thick Permian–Triassic marine gray clastics. Near the Kola Peninsula on the southern end of the profile, the sedimentary cover thins down to 3 km or less.

Wideangle deep seismic profiling for the first time demonstrated that the Paleozoic strata are the thickest in the Barents megabasin proper (up to 10 km in the future South Barents Basin). On the flanks of the megabasin, the Paleozoic thins down rapidly to 1–3 km. Up to 5 seismostratigraphic sequences have been recognized in the Paleozoic in some parts of the profile. The profile uniquely demonstrates the existence of a vast marine sedimentary basin during the Paleozoic. This fact is additionally supported by the increasingly open marine habit of sediments toward the center of the basin, the presence of Early Permian reefs on its paleoflanks, and the absence of synchronous carbonates in its deep-water central part.

The modeled heat flow values also attest to the continuity of the Paleozoic and underlying strata along this profile. On average, they do not differ much from the background values (the background value for this profile is 54 mW/m^2, as mentioned above) and range between 51 and 67 mW/m^2. Peak values along the profile are confined to the pinchouts of the clastic–carbonate sequence on the continental margin due to the structural effect of heat flow refraction in rocks with relatively lower thermal conductivities. We have no evidence for the existence of significant convective heat and mass transfer below the limit of seasonal temperature variations. Therefore, heat flow here is purely conductive, and its insignificant variations are attributable to structural geologic factors.

Also, the short ShGSP-3 profile is highly informative. It illustrates the junction between the Novaya Zemlya Archipelago and the eastern flank of the Ludlov–Lunin saddle [5]. Three blocks have been recognized within it, corresponding (from west to east) to the eastern flank of the megabasin, Admiralteiskii arch, and Sedov trough. The most complete sedimentary sequence was recorded on the eastern flank of the megabasin. Only the lower consolidated crust and a lenticular anomaly in the mantle have been identified here. A different situation was observed on the Admiralteiskii arch, where the sedimentary sequence is reduced. The second structural unit of the cover is only represented by the Lower Triassic (a well has been drilled here), and the third unit is probably restricted to the Devonian–Carboniferous. This attests to the possible existence of a vast uplift zone immediately west of Novaya Zemlya during the Early–Middle Paleozoic. It was only involved in subsidence by the Frasnian time. The Paleozoic sequence in the Sedov trough is more complete. Both eastern blocks adjacent to the Novaya Zemlya Archipelago are similar in that they both have a subcontinental type of crust and the dip of the Moho discontinuity beneath the archipelago.

Temperature and heat flow profiles here are typical of sedimentary cover thinning (pinchout) zones, as is clear from seismic data on the Admiralteiskii arch. Heat flow monotonously increases from the Ludlov–Lunin saddle (63–64 mW/m^2) toward the Admiralteiskii arch (68–70 mW/m^2), that is, increases by 10% along the profile. This is typical of areas, where sedimentary rocks with a low thermal conductivity give way to metamorphic rocks with higher thermal conductivity values.

Profile 38701 is interesting primarily due to the distinct differentiation of the lower structural unit of the sedimentary cover into four seismostratigraphic sequences. Here, stratified Riphean deposits were for the first time recognized within the vast West Kola trough between reflectors K_o and VI. The thickness of the Riphean in the deepest parts of the trough is as great as 4 km. The Riphean is blanketed by the distinctly stratified Cambrian–Silurian carbonates. Their thickness is uniform along the profile and does not exceed 1.5–2.0 km. The next graben (or synrift?) sequence is

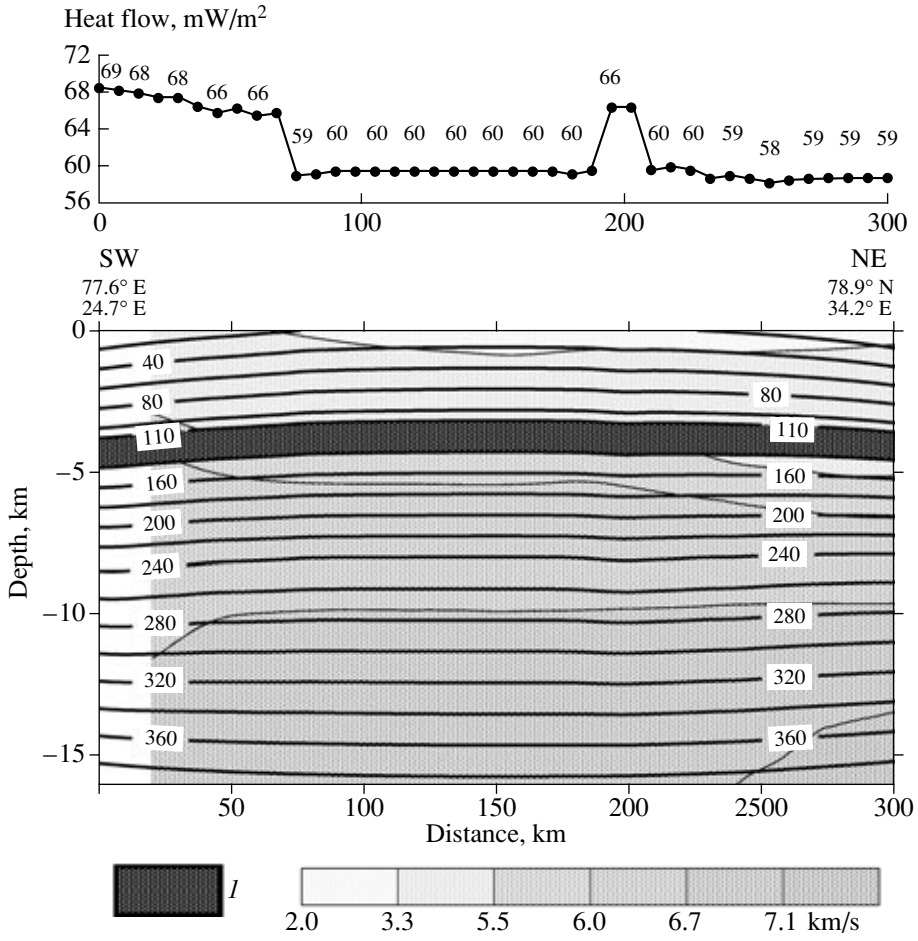

Fig. 6. Seismic tomography and temperature profiles along the MPV-83 line. See Fig. 5 for the legend.

dated as Early–Middle Devonian. The Devonian rocks in the central part of the trough exhibit sigmoid lateral accretion bodies with a thickness of up to 5–6 km in the deepest zones. This sequence is overlain by a thin transgressive blanket of post-Frasnian sediments. Their thickness does not exceed 1.5–2 km.

A narrow (10 km) deep-seated fault-bounded zone of deformed rocks has been detected at the boundary between the Kola–Kanin monocline and the West Kola trough. It is interpreted as the northwestern branch of the Timan–Pechora Baikalides. The Upper Riphean strata are broken by numerous Late Baikalian faults. Note that no block movements along these faults have been recorded.

The most complete sedimentary sequence can only be found within the trough, and this attests to its ancient origin. The cover sequence is reduced on adjacent highs (Kola–Kanin monocline and Murmansk massif), primarily due to the omission or abrupt thinning of the Riphean and Devonian graben complexes. This is also true of the thick Permotriassic sediments in the next structural unit, which accumulated in significant volumes in the West Kola trough.

The modeled geothermal sequence demonstrates the amazingly symmetrical temperature and heat flow distribution relative to the Kola–Kanin monocline and the Murmansk massif. The depressions surrounding these anticlinal structures exhibit lower heat flow values (up to 58–60 mW/m^2) than in the Kola–Kanin structure (68–69 mW/m^2). The thermal field exhibits a thermal dome pronounced in the interval 10–20 km. These specific features of geothermal fields result from heat flow perturbations in a setting of structural and thermal heterogeneity.

The structure of the western sector of the sea was studied on the basis of interpreted MPV-83, MPV-8, and 90243 DSS lines.

Line MPV-83 in its southwestern part crosses the Svalbard anteclise and the arch separating this structure from the Barents–North Kara megabasin and then crosses this megabasin along a Paleogene rift with a Neocomian–Eocene synrift unit at the base of the sedimentary fill. The thickness of the clastic–carbonate sequence is uniform along the whole trough and gently plunges from a depth of 3–4 km in the southwestern sector of the profile to a depth of 5–7 km in the north-

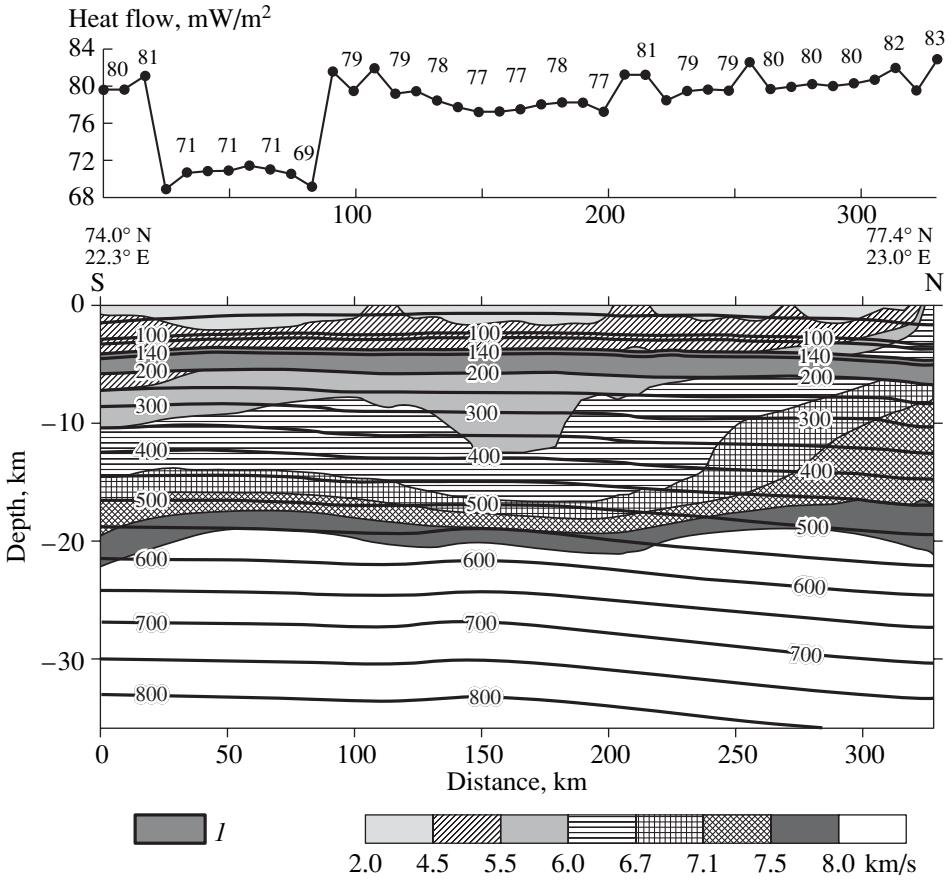

Fig. 7. Seismic tomography and temperature profiles along the 90243 line. See Fig. 5 for the legend.

eastern sector. We may suggest that the orientation of this profile along the strike of the main structural heterogeneities accounts for the subhorizontal pattern of seismic boundaries (Fig. 6).

As is well known, heat flow refraction takes place in the presence of contrasting thermal properties combined with structural–geologic heterogeneities, that is, deviations from the flatly parallel bedding. In this case, we observe a homogeneous heat flow along the profile (Fig. 6). The heat flow value is 59–60 MW/m^2 with insignificant (less than 10%) deviations from the background values within domal uplifts (intervals 0–50 and 180–230 km). This profile is only verified by one well, where actual temperature and heat flow values were measured. Therefore, the modeled heat flow values should be considered as approximate, although the relative heat flow variations along the profile can only be revised if seismic data are differently reinterpreted.

The N–S trending line 90243 is confined to the Svalbard anteclise (Fig. 7).

As is obvious from seismic tomography data, lower crustal layers with interval velocities of 6.7 to 7.5 km/s thicken and rise up northward, that is, toward the Svalbard Archipelago. Simultaneously, the thickness of the clastic sediments decreases. These factors exert different effects upon the thermal field. In case of their superposition, the heat flow along the profile remains virtually uniform (77–80 mW/m^2) except for the deep sedimentary basin with a clastic fill in the southern part of the profile, where heat flow drops down to 70 mW/m^2. For the reasons mentioned above, the reliability of modeled heat flow values in Fig. 7 cannot be guaranteed. The model data reflect only relative heat flow variations against the preset terminal conditions for this sequence.

The N–S profile MPV-8 is approximately 1000 km long and crosses the whole Barents megabasin. It has crossings with lines GSZ-76 and 89000, so the structural and geothermal modeling results from these profiles were compared in the crossings and demonstrated a close match.

Temperatures were calculated to a depth of 30 km, where they exceeded 700°C. The pattern of isotherms and heat flow profile reflect the configurations of the clastic and clastic–carbonate sequences, but spatial heat flow variations are insignificant in terms of absolute value. For example, heat flow varies within 55–65 mW/m^2 along this extensive profile, largely due to the lack of contrasts in thermal properties, the absence of pronounced structural heterogeneities, and the low sedimentation

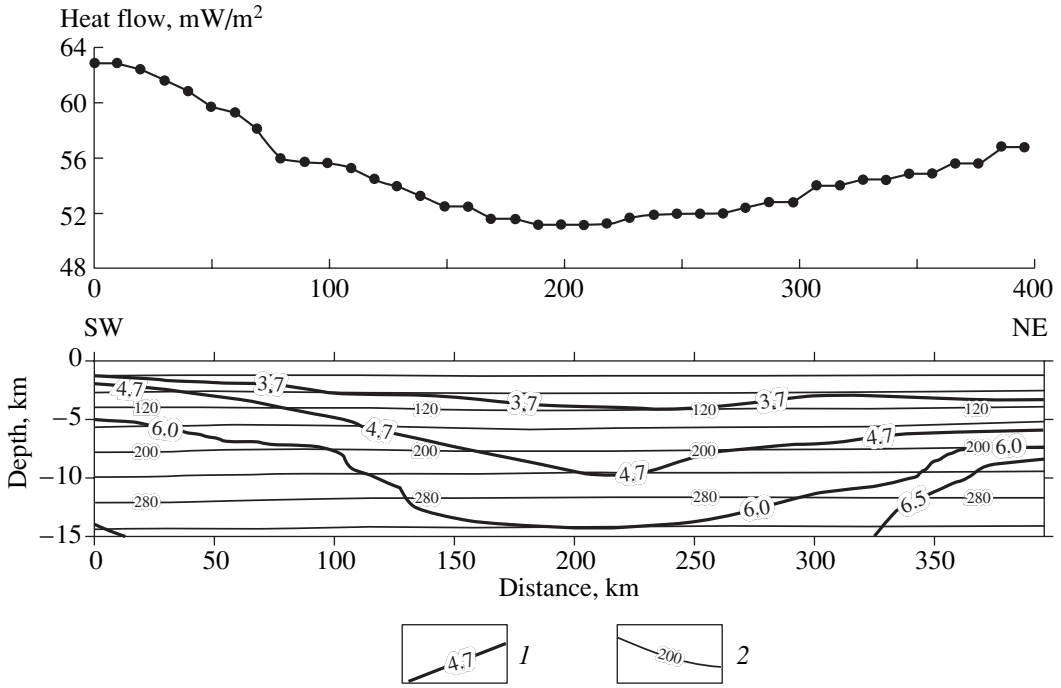

Fig. 8. Seismic and geothermal profiles of the Kara Sea along the 88434 line with a heat flow profile in the upper part. (*1*) Seismic boundaries and refractor velocities, km/s; (*2*) isotherms, °C.

rate. Heat flow values measured at three stations along the profile are 53, 62, and 68 mW/m^2 and almost completely coincide with the model values.

The structure of the South Kara basin was studied by reflection and refraction seismic and gravity surveys. The data obtained suggest that the depression is a Mesozoic rift with a relatively thin continental crust (26–30 km) and a highly differentiated basement surface structure. Major faults are distinctly listric, and displacements along them are as great as 3–6 km [4]. The principal structural features of the rift system were formed as a result of the consecutive detachment of large wedges and slices of consolidated crust along the fault zones that flatten downward and wane in the lower crust. Crustal stretching in the South Kara basin is about 20%, which is similar to the values of extension in the South Barents and North Sea rift basins. The extensional geodynamic regime is always accompanied by an increase in temperature and heat flow. These geothermal tendencies have been observed in the South Kara Basin.

The South Kara sedimentary basin is the offshore terminus of the West Siberia megabasin and exhibits the highest HC potential over the whole of Russia's Arctic shelf. The HC resources are harbored entirely in the Mesozoic and are represented largely by gas.

The crustal structure of the Kara Sea was described by 24 profiles obtained from deep seismic sounding along regional geotraverses (10 profiles) (Fig. 2) and interpreted seismic data acquired along short reflection lines (14 profiles) [13]. For each profile, deep temperatures were calculated using TERMGRAF software. Heat flow values measured in several offshore exploratory wells (73–76 mW/m^2 in the western and 53 mW/m^2 in the eastern part west of the Arctic Institute Archipelago) and in onshore wells on the western coast of the Yamal Peninsula (54–58 mW/m^2) and on Belyi Island (54–59 mW/m^2) (Fig. 2) were used as end values at the lower boundary. Modeling data for one profile are given in Fig. 8. The calculations were based on the thermal properties of crustal layers that were consistent with the registered refractor velocities (see table).

The structural pattern of the West Arctic region is a typical mosaic and cannot be modeled in two dimensions with an a priori systematic error of 10–15% as compared with a three-dimensional model of a domain with the same geothermal parameters and geometry. Taking this into account, we did not extrapolate the estimated deep temperatures beyond the profile site. To enable three-dimensional modeling, all the profile sites were combined in a single three-dimensional plot (Fig. 9) in latitude–longitude–depth coordinates.

The calculation accuracy was checked on the basis of two criteria, the match of modeled and measured (in wells) heat flow values and the match of temperatures at profile crossings. The error of isotherm occurrence depth, which was estimated by the least squares method, is ±150 m, which makes 0.5% if the calculation depth is up to 30 km.

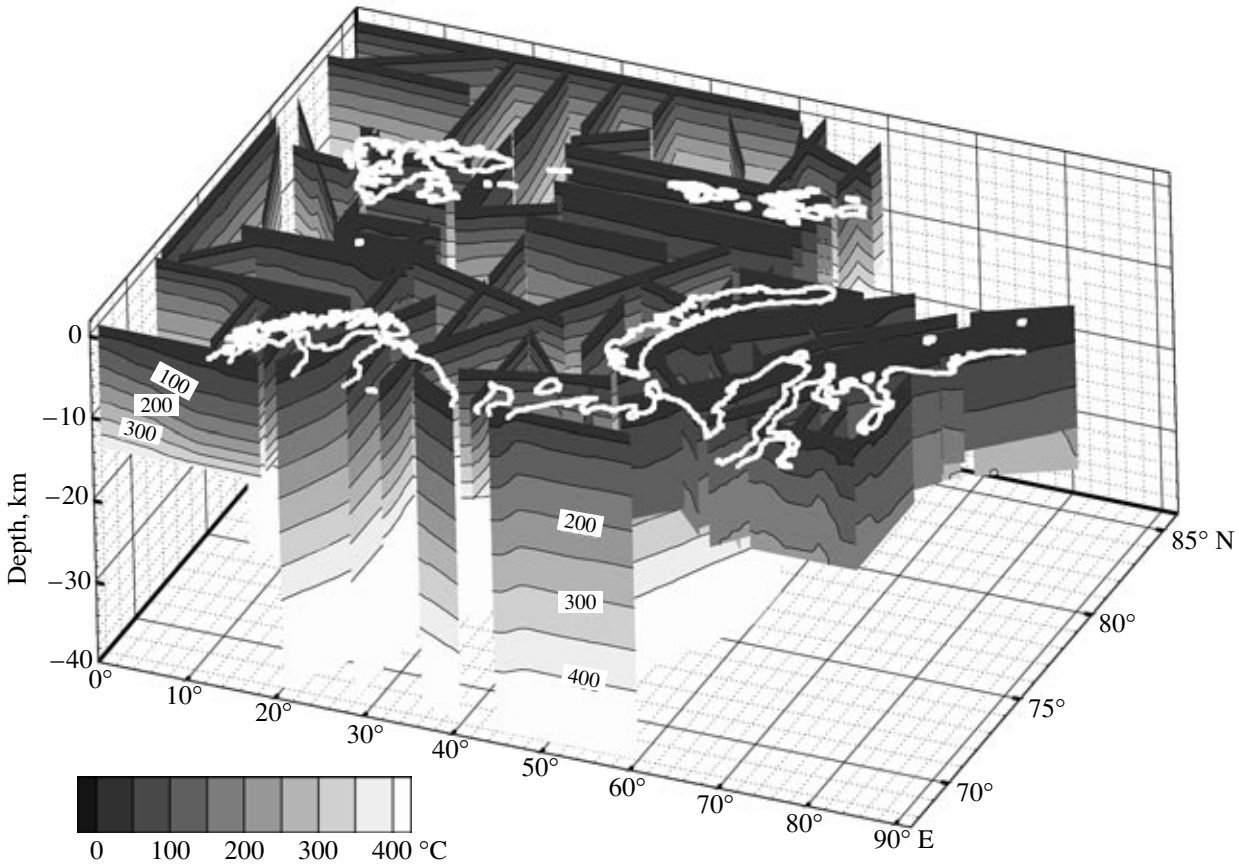

Fig. 9. Data obtained by 2D temperature modeling along geotraverses (Fig. 1) displayed on a 3D plot.

3D GEOTHERMAL MODELING

A specific feature of three-dimensional modeling is the estimation of temperatures and, consequently, all other geothermal parameters in the latitude–longitude–depth geometry for the whole region. Using the volumetric interpolation of the TECPLOT program, we obtained a three-dimensional temperature distribution pattern over the whole study interval (down to 35 km) and for the whole region (Fig. 10). A similar procedure was applied to obtain a three-dimensional heat flow distribution pattern. The program enables the depth slices of temperature and heat flow values and isothermal surfaces to be plotted for any interval.

Below is an analysis of the modeling data obtained.

The highest geothermal gradients have been detected in the southeastern and eastern sectors of the Barents Sea adjacent to the Kanin Peninsula, Kolguyev Island, and the Novaya Zemlya Archipelago (profiles MPV-84, GSZ-82, ShGSP-3, 38701) (Fig. 1). Naturally, they give rise to temperature anomalies in depth slices. The temperature anomalies relative to the background values range from +20°C at a depth of 3 km (against background temperatures of 90–100°C) to +40°C at a depth of 5 km (against background temperatures of 125–140°C). These anomalies, however, are due to the low thermal conductivity of the sequence caused by the landward thickening of the granite–metamorphic layer with a low thermal conductivity rather than elevated heat flow in the region. Nevertheless, the southeastern and eastern sectors of the Barents Sea are characterized by the rise of isothermal surfaces, including those that bound the oil-window temperature interval. This probably accounts for the concentration of the discovered oil and gas fields precisely around the thermal dome in the southeastern and eastern sectors of the sea, which is obvious from Fig. 11.

We do not exclude the possibility of discovering HC fields at greater depths in other parts of the Barents Sea. Using the same interpretation criteria for the occurrence of HC fields within the oil-window interval, HC discoveries can be anticipated at a depth of 6–8 km in the southwestern and western parts of the sea (MPV-8, GSZ-76, and 89000 lines) and at a depth of 5.5–7.0 km in its northwestern sector (MPV-83, 84103, and MPV-95 lines).

A similar situation probably exists in the Kara Sea: the thermal dome in the South Kara Basin spatially coincides with the large Rusanovskoye and Leningradskoye fields (Figs. 2, 10).

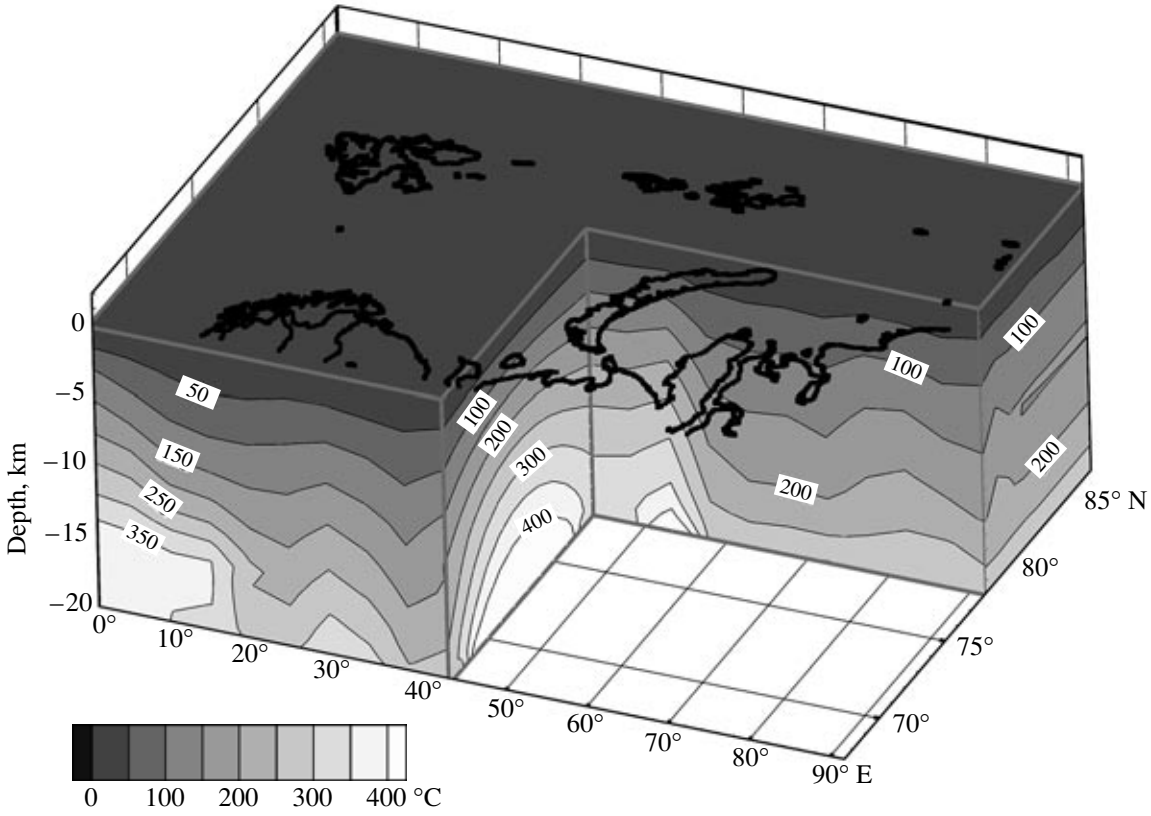

Fig. 10. 3D temperature plot of the West Arctic region.

As is obvious from the three-dimensional thermal model, isotherms rise over the whole depth interval (up to 15 km) in the South Kara Basin and thereby attest to the existence of a heat flow anomaly extending along the 66° E meridian from the central Baidaratskaya Estuary northward. This complies with the elevated (relative to the background) heat flow values measured in wells in the Rusanovskoye and Leningradskoye fields (73 and 76 mW/m^2, respectively) (Fig. 2). According to modeled data, temperatures at depths of 3, 4, and 5 km decrease by a relative value of 10°C east of this meridian, and the isotherms in the Belyi Ostrov depression (70° E) are already horizontal, which is typical of background geothermal conditions. The average heat flow value for the Yamal Peninsula is 53 mW/m^2—notably lower than the heat flow in the South Kara Basin.

A three-dimensional heat flow distribution model (Fig. 12) was obtained by special thermal data processing and then compared with the real heat flow estimates from downhole measurements. The regions with representative amounts of empirical data (the southeastern, eastern, and southwestern Barents Sea and southern Kara Sea) exhibit an almost perfect match between observed and model heat flow values at the top of the crust. In the Kanin–Kolguyev zone, for example, heat flow values are elevated according to downhole measurements (64–77 mW/m^2) and modeling results (60–80 mW/m^2), and another region with elevated heat flow values on the western flank of the Novaya Zemlya Range south of the ShGSP-3 line is also expressed in the three-dimensional heat flow model.

To summarize, we may state that the regions with a poorly known geothermal field, where elevated heat flow values were modeled, are likely to exhibit similar measured heat flow values in the future. One such region is the Svalbard anteclise between 75° and 80° N, and another is the North Kara Basin north of 76° N. The model plot clearly exhibits the decrease in heat flow with depth. This is due to the decrease in the proportion of the radiogenic component of heat flow with depth. As a result, heat flow values are reduced to 30–40 mW/m^2 at the base of this plot, as mentioned above in the description of the terminal conditions preset for modeling.

Three-dimensional geothermal modeling enables one to predict the depth interval of possible HC accumulation, in contrast to two-dimensional modeling, which prevents any extrapolations beyond the section line. Significant differences in estimates of petroleum potential based on geothermal data are possible for isometric rather than linear structures. For the isometric Barents–Kara platform, the depth to the oil window as estimated by two-dimensional modeling may differ by

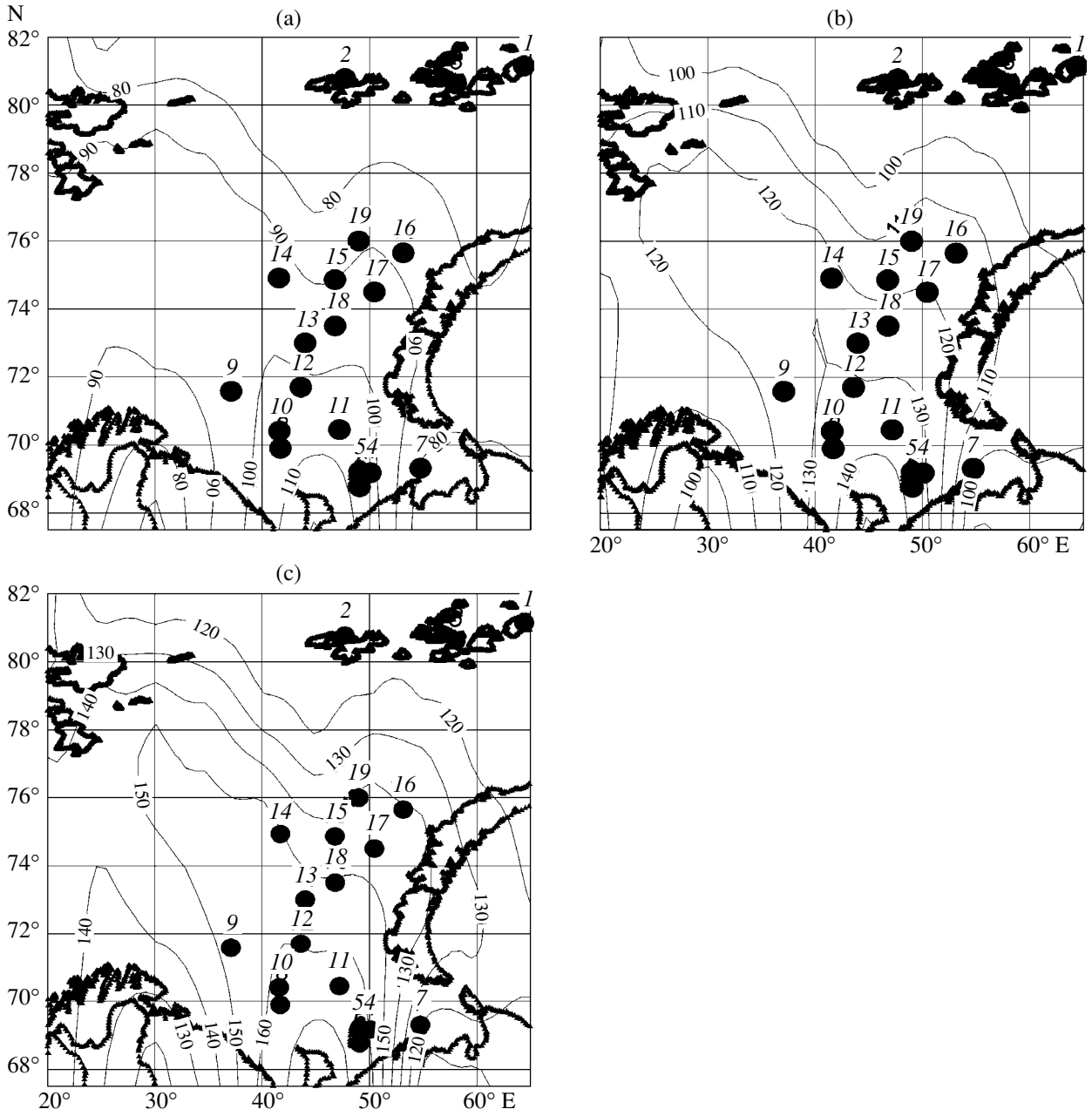

Fig. 11. Temperature distributions in the Barents Sea at a depth of 3 km (a), 4 km (b), and 5 km (c). Solid circles are productive wells; *1*—Severnaya, *2*—Nagurskaya, *3*—Kheisa, *4*—Peschanoozerskaya (oil), *5*—Izhimsko–Tarkskaya (oil), *6*—Burginskaya (gas), *7*—Severo-Gulyayevskaya (oil + gas), *8*—Murmanskaya (gas), *9*—Severo-Kil'dinskaya (gas), *10*—Severo-Murmanskaya (gas), *11*—Kurentsovskaya (oil), *12*—Arkticheskaya, *13*—Shtokmanovskaya-1 (gas + condensate), *14*—Fersmanovskaya, *15*—Ludlovskaya-1 (gas), *16*—Admiralteiskaya, *17*—Krestovaya, *18*—Ledovaya (gas), *19*—Luninskaya.

10–15% from estimates based on three-dimensional modeling. This fact does not require special proof, because it is well known from the classical works on the theory of thermal conductivity. Estimated difference variations within 5% are due to changes in thermal properties along the third spatial axis.

A specific feature of thermal tomographic modeling is the establishment of temperatures and, consequently, all the other geothermal parameters in the latitude–longitude–depth geometry for the whole region. This method enables temperature and heat flow distribution patterns, as well as isothermal surfaces, to be compiled for any depth slices.

The application of nonstationary geothermal modeling techniques to paleotemperature analysis in the lithosphere of the geologic past has shown that rifting in the southern Barents and Kara seas was of short duration, so the lithosphere did not thin down to the val-

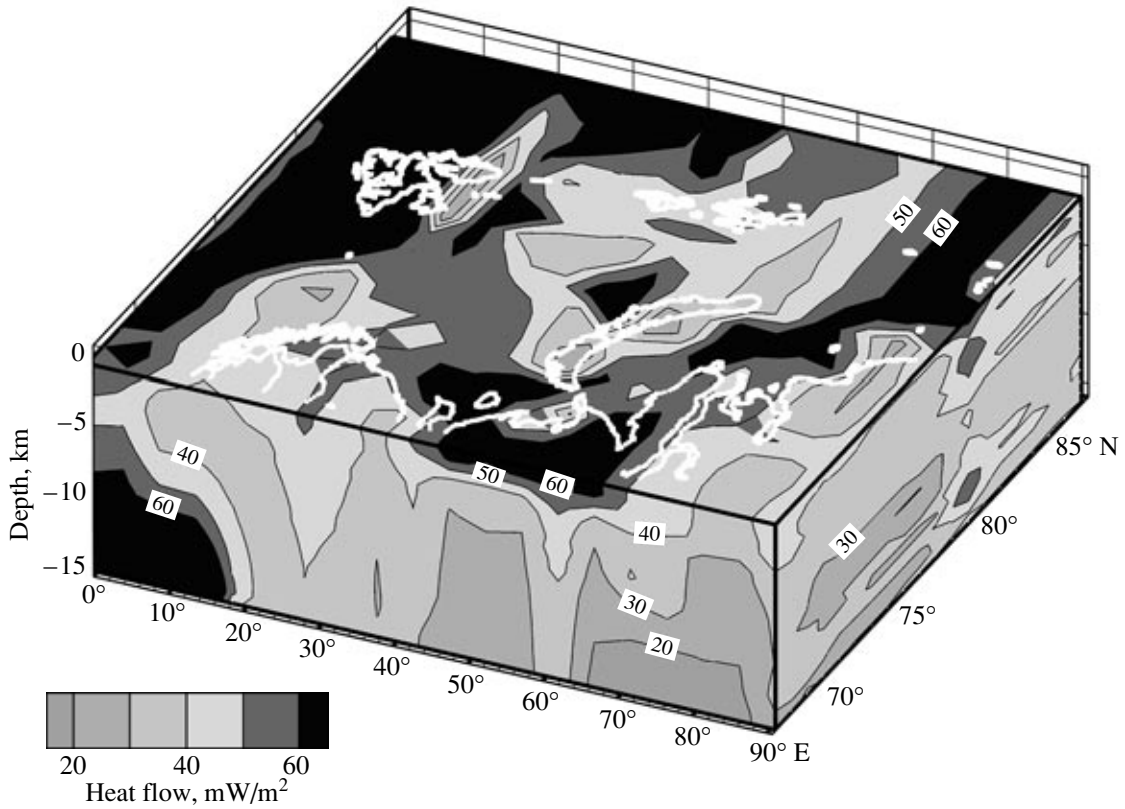

Fig. 12. Three-dimensional heat distribution plot.

ues typical of oceans. Therefore, the Middle and Late Paleozoic destruction of the Barents–Kara platform did not destroy the Proterozoic continental crust completely but led to its thinning and sagging. Thermal relaxation after this tectonic event rapidly led to the establishment of quasi-stationary background heat flow values typical of the other Paleozoic structures. Local zones of elevated temperature and heat flow values, as shown above, were formed in the stationary field as a result of structural geologic and thermal heterogeneities.

The West Arctic sea shelf shows a uniform tendency for the occurrence of large HC fields in the zones of high thermal potential. This fact can be used as an additional HC prospecting indicator on the Arctic shelf.

ACKNOWLEDGMENTS

This work was supported by the Russian Foundation for Basic Research (project no. 99-05-64801) and a grant within the Universities of Russia program.

REFERENCES

1. Arshavskaya, N.I., Comparison of Radiogenic Heat Flows in the Earth's Crust of the Baltic Shield and Kamchatka, in *Teplovye potoki iz kory i verkhnei mantii. Verkhnyaya mantiya* (Heat Flows from the Crust and the Upper Mantle. The Upper Mantle), Moscow: Nauka, 1973, no. 12, pp. 26–31.
2. Berezin, V.V. and Popov, Yu.A., Heat Flow of the Pechenga Structure, *Izv. Vyssh. Uchebn. Zaved., Geol. Razv.*, 1986, no. 13, pp. 105–108.
3. Berezin, V.V. and Popov, Yu.A., Geothermal Section of the Pechenga Structure, *Isv. Akad. Nauk SSSR, Fiz. Zemli*, 1988, no. 7, pp. 80–88.
4. Bogolepov, A.K., Murzin, R.R., and Khachatryan, S.S., Deep Structure of the East Barents and South Kara Rift Systems, *Mater. Kongressa "300 let rossiiskoi geologicheskoi sluzhbe,"* (Proc. of the Congress on the 300th Anniversary of the Russian Geologic Service), St. Petersburg: Vses. Geol. Inst., 2000, vol. 3, pp. 18–20.
5. Verba, M.L. and Sharov, N.V., *Sostoyanie izuchennosti i osnovnye problemy glubinnogo stroeniya Barentsevskogo regiona*, (Exploration Maturity and Deep Structure of the Barents Sea Region), Apatity: Geol. Inst., Kol'sk. Nauchn. Tsentr Ross. Akad. Nauk, 1988, part 1, pp. 11–41.
6. Zorin, Yu.A. and Osokina, S.V., Model of the Nonstationary Crustal Temperature Field in the Baikal Rift Zone, *Isv. Akad. Nauk SSSR, Fiz. Zemli*, 1981, no. 7, pp. 17–25.
7. *Metodicheskie i eksperimental'nye osnovy geotermii* (Methodological and Experimental Fundamentals of Geothermometry), Moscow: Nauka, 1983.
8. Milanovskii, E.E., *Riftovye zony kontinentov* (Continental Rift Zones), Moscow: Nedra, 1976.

9. Milanovskii, S.Yu., Kremenetskii, A.A., and Ovchinnikov, L.N., Geothermal Surveys and Crustal Heat Generation Model for the Northeastern Baltic Shield, in *Geokhimiya glubinnykh porod* (Geochemistry of Abyssal Rocks), Moscow: Nauka, 1986, pp. 131–149.
10. *Petrofizika: Spravochnik. Kn. 1. Gornye porody i poleznye iskopaemye*, (Petrophysics: A Handbook, vol. 1: Rocks and Mineral Resources), Dortman, N.B., Ed., Moscow: Nedra, 1992.
11. Podgornykh, L.V. and Khutorskoi, M.D., Thermal Evolution of the Lithosphere in the Junction Zone between the Baltic Shield and the Barents Sea Plate, *Fiz. Zemli*, 1998, no. 3, pp. 56–65.
12. Podgornykh, L.V., Khutorskoi, M.D., Gramberg, I.S., and Leonov, Yu.G., Three–Dimensional Geothermal Model of Kara Sea Shelf and Its Predicted Petroleum Potential, *Dokl. Akad. Nauk*, 2001, vol. 380, no. 2, pp. 228–232.
13. Poselov, V.A., Pavlenkin, A.D., and Butsenko, V.V., Structure of the Lithosphere from DSS Geotraverses in the Arctic, in *Geologo–geofizicheskie kharakteristiki litosfery Arkticheskogo regiona* (Geologic–Geophysical Characteristics of the Lithosphere in the Arctic Region), St. Petersburg: Vseross. Nauch.–Issled. Inst. Okeangeologii, 1996, issue 1, part 2, pp. 145–155.
14. Ustritskii, V.I. and Khramov, A.N., Geologic History of the Arctic in Terms of Plate Tectonics, in *Morya Sovetskoi Arktiki* (Soviet Arctic Seas), Leningrad: Nedra, 1984, pp. 253–265.
15. Khutorskoi, M.D., *Geotermiya Tsentral'no–Aziatskogo skladchatogo poyasa* (Geothermometry of the Central Asian Foldbelt), Moscow: Izd. RUDN, 1996.
16. Khutorskoi, M.D. and Podgornykh, L.V., A Volumetric Model of the Geothermal Field of the Barents Sea Region, *Dokl. Akad. Nauk*, 2001, vol. 377, no. 1, pp. 265–269.
17. Tsybulya L.A. and Levashkevich V.G. *Teplovoe pole Barentsevomorskogo regiona.* (Heat Flow Field of the Barents Sea Region), Apatity: Geol.Tsentr, Kol'sk. Nauchn. Tsentr Ross. Akad. Nauk, 1992.
18. Erinchik, Yu.M. and Mil'shtein, E.D., *Rifeiskii riftogenez tsentral'noi chasti Vostochno–Evropeiskoi platformy*, (Riphean Rifting in the Central Part of the East European Craton), St. Petersburg: Vses. Geol. Inst., 1995.
19. Bullard, E.S. and Day, A., The Flow of Heat through the Floor of the Atlantic Ocean, *J. Geophys. Res.*, 1961, vol. 27, pp. 282–292.
20. Crough, S.T. and Thompson, G.A., Numerical and Approximate Solution for Lithospheric Thickening and Thinning, *Earth Planet. Sci. Lett.*, 1976, vol. 31, pp. 397–402.
21. Fairhead, J.D., The Structure of the Lithosphere beneath the Eastern Rift, East Africa, Deduced from Gravity Studies, *Tectonophysics*, 1976, vol. 30, pp. 269–298.
22. Khutorskoy, M.D., Fernandez, R., Kononov, V.I., *et al.*, Heat Flow through the Sea Bottom around the Yucatan Peninsula, *J. Geophys. Res.*, 1990, vol. 95, no. B2, pp. 1223–1237.
23. Lachenbruch, A.H. and Marshall, B.V., Heat Flow and Water Temperature Fluctuations in the Denmark Strait, *J. Geophys. Res.*, 1968, vol. 73, no. 18, pp. 756–761.